Small-Signal Stability Analysis of Grid-Connected Converter under Different Grid Strength Cases

Dimitropoulos, Dimitrios; Wang, Xiongfei; Blaabjerg, Frede

Published in:
Proceedings of the 2022 IEEE 13th International Symposium on Power Electronics for Distributed Generation Systems (PEDG)

DOI (link to publication from Publisher):
10.1109/PEDG54999.2022.9923291

Publication date:
2022

Document Version
Accepted author manuscript, peer reviewed version

Small-Signal Stability Analysis of Grid-Connected Converter under Different Grid Strength Cases

Dimitrios Dimitropoulos
AAU Energy
Aalborg University
Aalborg, Denmark
ddi@energy.aau.dk

Xiongfei Wang
AAU Energy
Aalborg University
Aalborg, Denmark
xwa@energy.aau.dk

Frede Blaabjerg
AAU Energy
Aalborg University
Aalborg, Denmark
fbl@energy.aau.dk

***Abstract*—Nowadays, the need for a more sustainable power system is leading to the utilization of power-electronic converter technology (eg. in wind and PV applications); however, stability issues in converter-based power systems have been under discussion for a while. In this paper, a small-signal model is developed to analyze the control dynamics of grid-connected power converters and investigate the impact of control gains on the system stability. The dynamics are expressed using a non-linear state-space modeling system and the sensitivity level of this model is studied in details. Linearization is implemented around the equilibrium points of the system and stability is assessed through its eigenvalue analysis. Time-domain simulations are performed to verify the accuracy of the model and corresponding FFT analysis are obtained when instability occurs in order to validate the small-signal analysis model.**

***Index Terms*—power electronics, small-signal modelling, grid-following converter, vector current control, eigenvalue analysis, stability analysis, time-domain analysis, FFT analysis**

I. Introduction

In the last years, there has been a large increase in the volume of wind turbines installed in power systems. Europe had 236 GW of wind energy capacity in 2021, the energy generated by wind power was equal to 437 TWh in 2021 and accounted for 15% of the EU-28 consumed electricity [1]. This high level of renewable penetration to the main grid is leading the evolution of power systems, moving from synchronous machines dominated system to become converter-based system. In that way more flexibility is achieved and maybe also higher efficiency can be obtained; however, challenges to the stability of the system will also arise as more components are connected to the power system [2].

In case of analyzing small disturbances, small-signal modeling is applied and a state-space model of the whole system can be developed for evaluating the robustness and the dynamic phenomena caused by the system's control structures [3]. The state-space model of a grid-connected inverter is developed and analyzed in [4] based on proportional-integral (PI) controllers of the current and Park's transformation, but the system is not linearized around its equilibrium points and eigenvalue analysis results are not provided. The eigenvalue trajectories of the system can be observed in [5]–[9] and [12], as a linearization of the state-space model is implemented. In [5] and [7]–[9] though, a digital time delay is not considered, whereas in [6] and [12] the phased-locked loop (PLL) coupling to the grid and the corresponding dynamics are not investigated either. In [10], a 1^{st} order Padé approximation is used to model the time delay, but a higher order of this approximation is more accurate [11]. Therefore, this paper presents the development of a linearized small-signal model of a Voltage Source Converter (VSC) connected to the grid with an LC filter, where the dynamic relations between the PLL and the grid, as well as the impact of time delay, are considered. In this work, the sensitivity of control gains for the small-signal model's stability is emphasized for different grid strength cases. The analysis is validated by simulations in the time domain as well as in the frequency domain through Fast-Fourier Transformation (FFT).

II. Model Description

In state-space modeling, the model developed should represent all the dynamics of the converter in the frequency range of interest and also allow coupling models of the distribution network. A complete small-signal wind turbine model should also include the control system for the power electronic converter circuit. This consists of the PLL, the Park (abc–dq) transformations, the current and voltage controllers, the digital time delay in sampled systems as well as any low-pass filters applied to feedback or to the control signals.

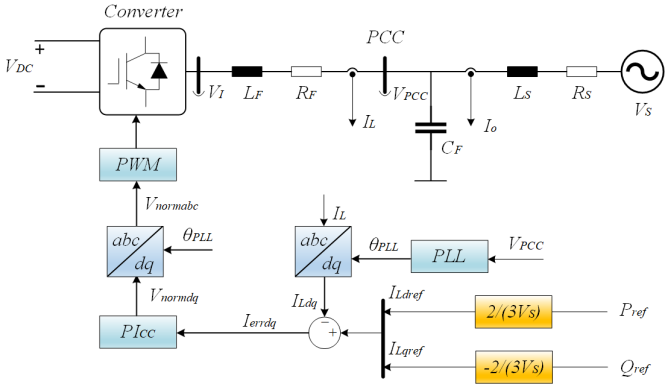

Fig. 1. Control structure of an LC-filtered grid-following converter connected to the grid.

A state-space model of the system is developed then; it is described by (1) and consists of nonlinear state equations that describe the different control dynamics. These equations correspond to different components of the system, and the state-space model of the system is the result of combining the individual state-space models of the system components.

$$\begin{aligned} \dot{x} &= Ax + R(x,u) \\ y &= S(x,u) \end{aligned} \tag{1}$$

The structure of the system addressed in this work is depicted in Fig. 1. It entails a grid-following converter, which adopts vector current control. The synchronization of the converter to the grid is achieved by a PLL. The active and reactive power – from which the reference output current is calculated – are regulated to follow the corresponding reference values through open-loop control; this is a sufficient method, because an ideal converter is assumed. In addition, the inverter is assumed to be provided with a stable DC link voltage in this case.

A. Phase-Locked Loop (PLL)

The control structure of PLL is shown in Fig. 2. The q-axis component voltage V_{PCCq} at the Point of Common Coupling (PCC) is selected as the input to the PLL, and the PI controller outputs the angular speed of the PCC voltage ω_{PLL}. The voltage V_{PCCq} is regulated to zero due to the PI control; thus, the PCC voltage can be aligned with the d-axis.

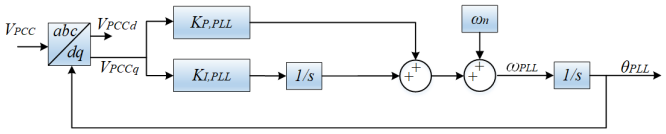

Fig. 2. Control structure of the used PLL in Fig. 1

The state variable of the PLL are

$$x_1 = \begin{bmatrix} \theta_{\mathrm{PLL}} & \Phi_{\mathrm{PLL}} \end{bmatrix} \tag{2}$$

where $\Phi_{\mathrm{PLL}}=\int V_{PCCq}\mathrm{dt}$.

The differential equations of the PLL are the following

$$\dot{\theta}_{\mathrm{PLL}} = K_{\mathrm{I,PLL}}\Phi_{\mathrm{PLL}} + K_{\mathrm{P,PLL}}V_{\mathrm{PCCq}} + \omega_{\mathrm{n}} \tag{3}$$

$$\dot{\Phi}_{\mathrm{PLL}} = V_{\mathrm{PCCq}} \tag{4}$$

B. Current Controller

The Current Control loop, which is shown in Fig. 3, regulates the converter output current by generating a proper output voltage reference. From Fig. 3, the following equations regarding the output of the current controller can be obtained as:

$$\begin{aligned} V_{\mathrm{normd}} = \frac{1}{V_{\mathrm{DC}}} \big(& V_{\mathrm{PCCd}} - \omega_{\mathrm{PLL}} L_{\mathrm{F}} I_{\mathrm{Lq}} \\ & + K_{\mathrm{P,d}} I_{\mathrm{errd}} + K_{\mathrm{I,d}} q_{\mathrm{errd}} \big) \end{aligned} \tag{5}$$

$$\begin{aligned} V_{\mathrm{normq}} = \frac{1}{V_{\mathrm{DC}}} \big(& V_{\mathrm{PCCq}} + \omega_{\mathrm{PLL}} L_{\mathrm{F}} I_{\mathrm{Ld}} \\ & + K_{\mathrm{P,q}} I_{\mathrm{errq}} + K_{\mathrm{I,q}} q_{\mathrm{errq}} \big) \end{aligned} \tag{6}$$

where q_{errdq} represents the integrators of the current controller.

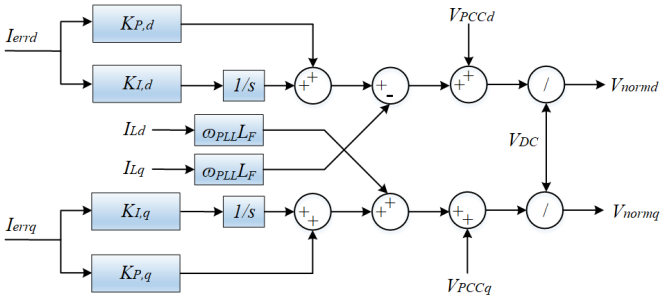

Fig. 3. Control structure of the current controller ($\mathrm{PI_{cc}}$) in Fig. 1

The error current is derived by the d- and q- axis current references from which the measured converter currents are subtracted. The reference currents can be calculated from the desired active and reactive power, as shown in the following equations, where V_S is the nominal voltage of the grid.

$$I_{\mathrm{Ldref}} = \frac{P_{\mathrm{ref}}}{1.5V_{\mathrm{S}}} \tag{7}$$

$$I_{\mathrm{Lqref}} = -\frac{Q_{\mathrm{ref}}}{1.5V_{\mathrm{S}}} \tag{8}$$

The state variables of the current controller are

$$x_2 = \begin{bmatrix} q_{\mathrm{errd}} & q_{\mathrm{errq}} \end{bmatrix} \tag{9}$$

The differential equations of the current controller are the following

$$\dot{q}_{\mathrm{errd}} = I_{\mathrm{Ldref}} - I_{\mathrm{Ld}} \tag{10}$$

$$\dot{q}_{\mathrm{errq}} = I_{\mathrm{Lqref}} - I_{\mathrm{Lq}} \tag{11}$$

C. Time Delay

The time delay plays an important role on the digital control system. It is here designed based on a 3^{rd} order Padé approximant, which approximates the delay in the plant by utilizing the following transfer function.

$$e^{-\mathrm{T_d}s} = \frac{\left(b_0 + b_1 T_{\mathrm{d}} s + \ldots + b_{\mathrm{l}} \left(T_{\mathrm{d}} s\right)^{\mathrm{l}}\right)}{\left(a_0 + a_1 T_{\mathrm{d}} s + \ldots + a_{\mathrm{k}} \left(T_{\mathrm{d}} s\right)^{\mathrm{k}}\right)} \tag{12}$$

where l and k are the order of Padé approximation, $a_{\mathrm{j}} = \frac{(l+k-j)!k!}{j!(k-j)!}$, $j = 0, \ldots, k$ and $b_{\mathrm{i}} = (-1)^{\mathrm{i}} \frac{(l+k-i)!l!}{i!(l-i)!}$, $i = 0, \ldots, l$. Also, T_{d} is the delay time which is typically 1.5 times the sampling period.

The state variables of the time delay are

$$x_3 = \begin{bmatrix} x_{\mathrm{del,1d}} & x_{\mathrm{del,2d}} & x_{\mathrm{del,3d}} & x_{\mathrm{del,1q}} & x_{\mathrm{del,2q}} & x_{\mathrm{del,3q}} \end{bmatrix} \tag{13}$$

The differential equations of the digital time delay are the following

$$\dot{x}_{\mathrm{del,1dq}} = 0x_{\mathrm{del,1dq}} + 1x_{\mathrm{del,2dq}} + 0x_{\mathrm{del,3dq}} \tag{14}$$

$$\dot{x}_{\mathrm{del,2dq}} = 0x_{\mathrm{del,1dq}} + 0x_{\mathrm{del,2dq}} + 1x_{\mathrm{del,3dq}} \tag{15}$$

$$\dot{x}_{\text{del,3dq}} = -\frac{120}{T_d^3}x_{\text{del,1dq}} - \frac{60}{T_d^2}x_{\text{del,2dq}} - \frac{12}{T_d^1}x_{\text{del,3dq}} + V_{\text{normdq}} \tag{16}$$

D. LC Filter and Grid-Side Impedance

The model entails an LC filter - as shown in Fig. 4 - to suppress harmonics from the PWM modulation of the converter as well as high harmonics originated by the converter. The corresponding state-space subsystem also includes the grid impedance dynamics, and its state variables are

$$x_4 = \begin{bmatrix} I_{\text{Ld}} & I_{\text{Lq}} & V_{\text{PCCd}} & V_{\text{PCCq}} & I_{\text{od}} & I_{\text{oq}} \end{bmatrix} \tag{17}$$

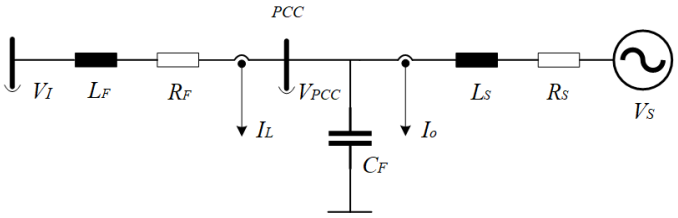

Fig. 4. LC filter and grid impedance circuit in Fig. 1

The VSC bridge voltage V_I is the output of the time delay subsystem, and it is calculated as given below

$$V_{\text{Id}} = V_{\text{DC}}\left(\frac{240}{T_d^3}x_{\text{del,1d}} + 0x_{\text{del,2d}} + \frac{24}{T_d^1}x_{\text{del,3d}} - V_{\text{normd}}\right) \tag{18}$$

$$V_{\text{Iq}} = V_{\text{DC}}\left(\frac{240}{T_d^3}x_{\text{del,1q}} + 0x_{\text{del,2q}} + \frac{24}{T_d^1}x_{\text{del,3q}} - V_{\text{normq}}\right) \tag{19}$$

Thus, the differential equations that describe the dynamics of the LC filter and grid impedance are given below

$$\dot{I}_{\text{Ld}} = -\frac{R_F}{L_F}I_{Ld} + \left(-\frac{1}{L_F}V_{PCCd}\right) + \omega_{\text{PLL}}I_{Lq} + \frac{1}{L_F}V_{\text{Id}} \tag{20}$$

$$\dot{I}_{\text{Lq}} = -\frac{R_F}{L_F}I_{Lq} + \left(-\frac{1}{L_F}V_{PCCq}\right) - \omega_{\text{PLL}}I_{Ld} + \frac{1}{L_F}V_{\text{Iq}} \tag{21}$$

$$\dot{V}_{\text{PCCd}} = \frac{1}{C_F}I_{Ld} + \left(-\frac{1}{C_F}I_{od}\right) + \omega_{\text{n}}V_{PCCq} \tag{22}$$

$$\dot{V}_{\text{PCCq}} = \frac{1}{C_F}I_{Lq} + \left(-\frac{1}{C_F}I_{oq}\right) - \omega_{\text{n}}V_{PCCd} \tag{23}$$

$$\dot{I}_{\text{od}} = \frac{1}{L_S}V_{PCCd} + \left(-\frac{R_S}{L_S}I_{od}\right) + \left(-\frac{1}{L_S}V_{Sd}\right) + \omega_{\text{n}}I_{oq} \tag{24}$$

$$\dot{I}_{\text{oq}} = \frac{1}{L_S}V_{PCCq} + \left(-\frac{R_S}{L_S}I_{oq}\right) + \left(-\frac{1}{L_S}V_{Sq}\right) - \omega_{\text{n}}I_{od} \tag{25}$$

III. Small-Signal Linearization and Stability Analysis

The main type of small-signal instability seen in a grid-following converter is the sideband oscillation of the grid fundamental frequency. The stability of the converter-based system will be evaluated after the possible equilibrium points are obtained from the linearized state-space model. The local stability of the system is assessed by a linear approximation of the state-space model system which is:

$$\dot{x} = Ax \tag{26}$$

where A is the Jacobian matrix that entails the partial derivatives of the system at fixed points. The fixed points are determined by solving $\dot{x} = 0$ for all state equations of the system. In this work, the eigenvalue sensitivity is applied to evaluate the small-signal stability. This sensitivity is based on the control parameters of the system's control structures, which are varied to identify the magnitude which is correlated to instability. The small-signal model is first tested for the current controller's model accuracy and for different grid strength cases, starting from a strong grid case scenario where Short-Circuit Ratio (SCR) is equal to 15 and ending up with a weak grid case scenario where SCR is equal to 1.5.

TABLE I
System and Default Control Parameters

	Description	Value
V_S	Grid Phase Voltage	311 V
V_{DC}	DC Link Voltage Reference	800 V
L_F	Filter Inductance	3 mH
R_F	Filter Resistance	0.1 Ω
C_F	Filter Capacitance	10 μF
f_{sw}	Switching Frequency	20 kHz
f_S	Sampling Frequency	20 kHz
P_{ref}	Nominal Active Power	30 kW
Q_{ref}	Reactive Power	0 kVAR
K_{I0}	Default Integral Gain of Current Control	666.7
K_{P0}	Default Proportional Gain of Current Control	33.3
$K_{I,PLL0}$	Default Integral Gain of PLL	4.1672
$K_{P,PLL0}$	Default Proportional Gain of PLL	0.1637

In Fig. 5, the eigenvalue analysis of the small-signal model is presented for the system and the current control parameters given in Table I. The design target of the default PI current controller is to regulate the bandwidth of the current closed loop at $1/20$ of the switching frequency; the default bandwidth of PLL is 11.77 Hz. The grid inductance L_S is specified to give the corresponding SCR, and the grid resistance R_S is assumed equal to zero The controller gains are varied from 0.1 (deep blue) to 10 (red) times the default value of the controller and the eigenvalues pair of instability are shown, where the corresponding critical gain and critical frequency are underlined. Based on the movements of the eigenvalue trajectories, the system becomes unstable as the proportional gain of the current controller increases. The critical frequency is equal to approximately 1/6 of the switching frequency f_{sw} in all test cases.

Then the weak grid case is selected for analysis (SCR equal to 1.5) to perform the eigenvalue analysis for the PLL control

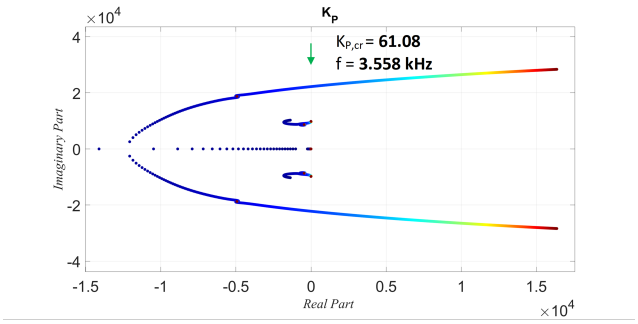

(a) SCR equal to 15

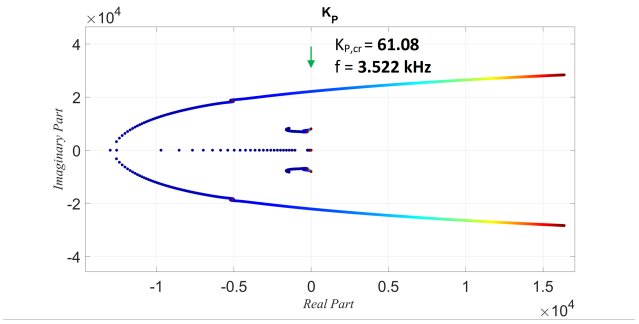

(b) SCR equal to 10

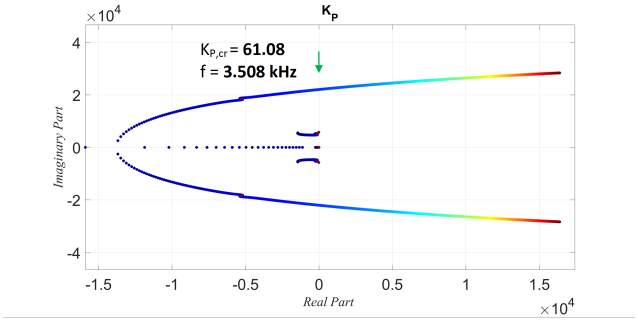

(c) SCR equal to 5

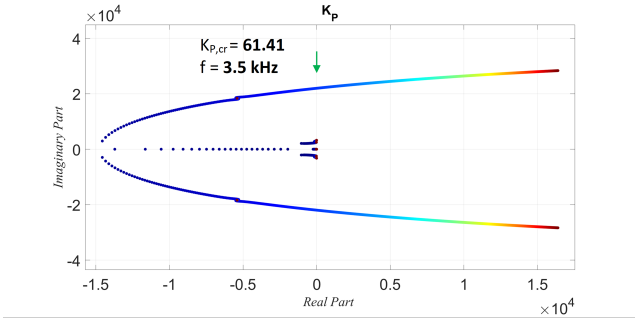

(d) SCR equal to 1.5

Fig. 5. Eigenvalue trajectories for variations in proportional gain of current controller (K_P) for different grid strength cases. K_P is varied from 0.1 (blue) to 10 (red) times K_{P0}. Green arrow means instability.

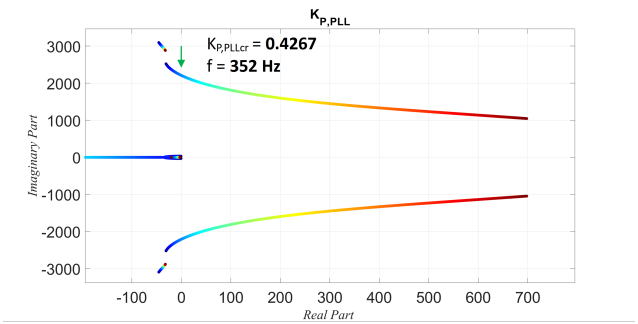

(a) $K_{P,PLL}$ is varied from 0.1 (blue) to 10 (red) times $K_{P,PLL0}$

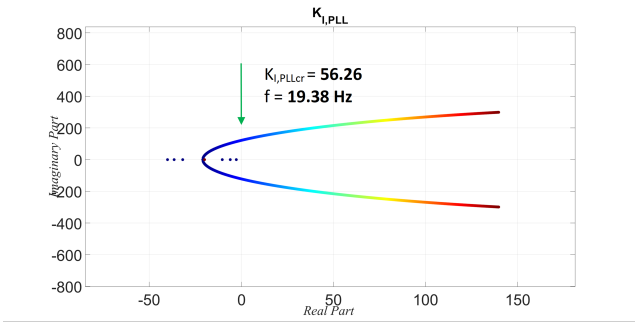

(b) $K_{I,PLL}$ is varied from 0.1 (blue) to 100 (red) times $K_{I,PLL0}$

Fig. 6. Eigenvalue trajectories for variations in PLL gains ($K_{P,PLL}$ and $K_{I,PLL}$) for weak grid case scenario (SCR equal to 1.5). Green arrow means instability.

parameters and the eigenvalues pair where instability is first observed is pointed out. $K_{P,PLL}$ and $K_{I,PLL}$ are varied and the eigenvalue trajectories are shown in Fig. 6; both controller gains lead to instability as being increased, since the PLL bandwidth is also increased.

IV. Simulation Results

In order to validate the small-signal model dynamic response, time-domain simulations have been carried out by using MATLAB Simulink and PLECS Blockset. The circuit and control parameters are the same as in the small-signal model and they are shown in Table I. Step changes are applied to the current control parameters at $t = 2$ seconds while the system is stable. The controller gains then obtain the values that critically impact the system's stability, and the inductor current in the dq-frame is utilized to demonstrate the instability cases in Fig. 7. FFT analysis is implemented when the system becomes unstable in order to identify the dominant frequency and compare it with the critical frequency of the corresponding small-signal model.

The simulation results show that there is a close match between them and the corresponding stability analysis results of the small-signal analysis shown in Fig. 5. Then, the time domain simulation regarding the sensitivity of the PLL control parameters was implemented when the SCR is equal to 1.5; the PLL bandwidth is increased from 11.77 Hz (default PLL

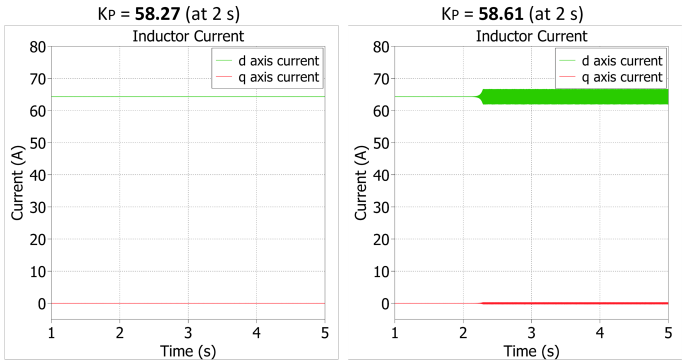

(a) SCR equal to 10 - Time domain analysis

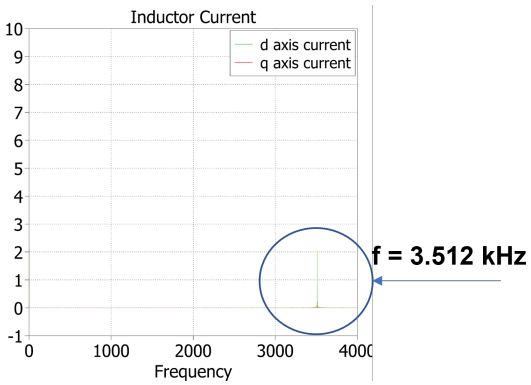

(b) SCR equal to 10 - FFT Analysis

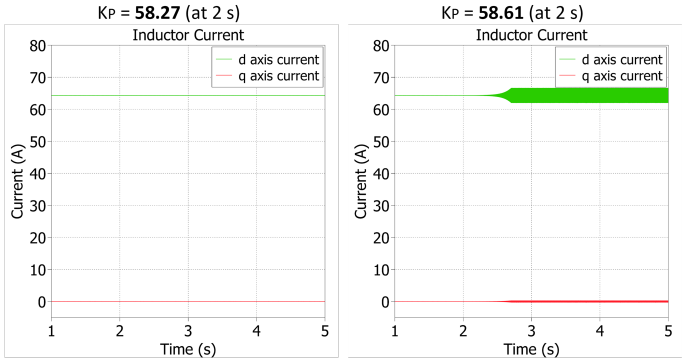

(c) SCR equal to 5 - Time domain analysis

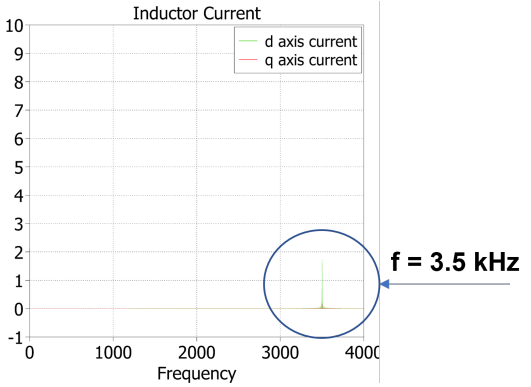

(d) SCR equal to 5 - FFT Analysis

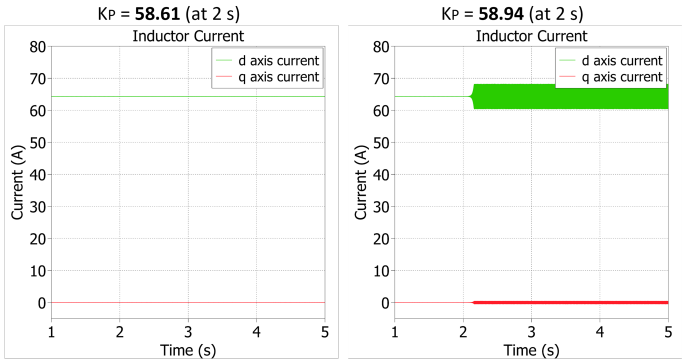

(e) SCR equal to 1.5 - Time domain analysis

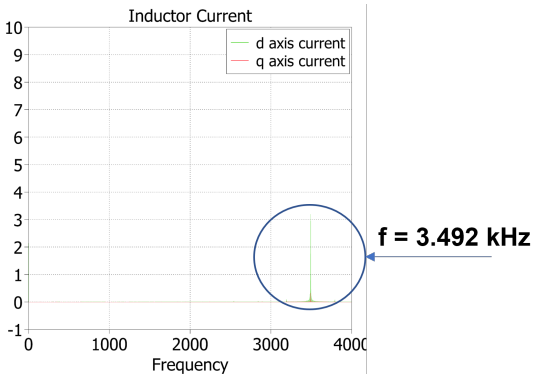

(f) SCR equal to 1.5 - FFT Analysis

Fig. 7. Time-domain simulations - inductor current for different grid strength cases and changes in K_P at t=2 sec

design) to 22.6 Hz and 34.1 Hz for step change in $K_{P,PLL}$ and $K_{I,PLL}$ respectively. The simulation results that correspond to the stability analysis results of the small-signal model in Fig. 6 are shown in Fig. 8 and verify the eigenvalue trends shown in the small-signal model results with a high accuracy.

V. Conclusion

The large penetration of converter-based generation leads to a need of further study of the converter control in order to understand the stability trends. This paper implements state-space modelling of the non-linear system of a VSC connected to the grid with an LC filter. The impacts of the PLL dynamics, current control dynamics, LC filter and digital time delay are considered in the structure of the small-signal model and a detailed small-signal model using state equations is analyzed for all system components in detail. The eigenvalue trajectories are obtained, and the eigenvalue trends are assessed based on the time-domain simulations and FFT analysis when the system becomes unstable. Based on this assessment, there is a close match between the obtained small-signal, time-domain and FFT analysis results for the different grid strength test cases, and this provides the developed small-signal model

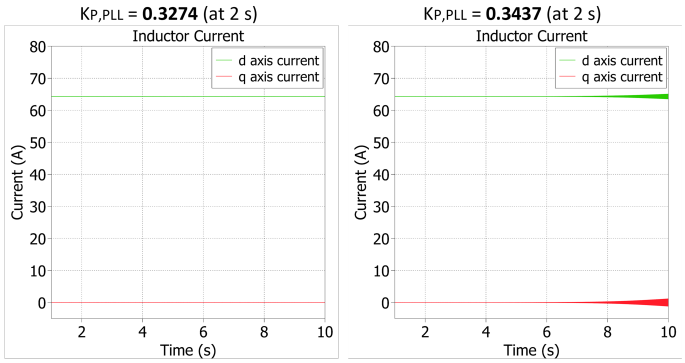

(a) Step change of $K_{P,PLL}$

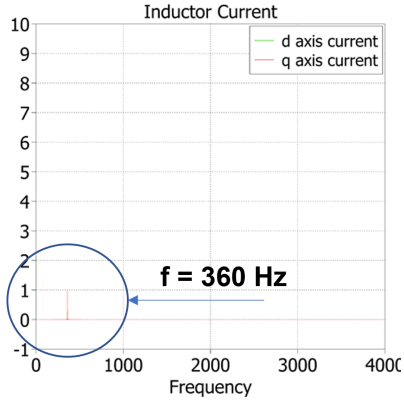

(b) FFT Analysis after a step change of $K_{P,PLL}$

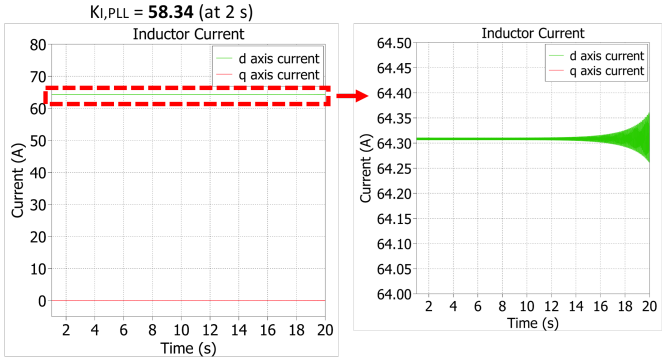

(c) Step change of $K_{I,PLL}$ - figure is maximized on the right side

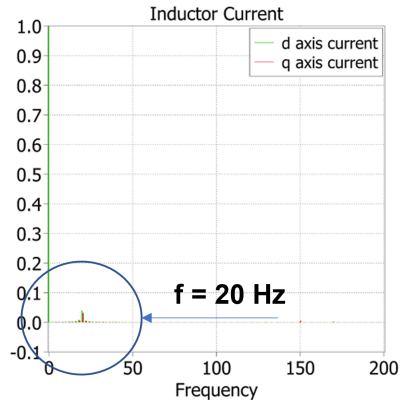

(d) FFT Analysis after a step change of $K_{I,PLL}$

Fig. 8. Time-domain simulations - output current when changes in the PLL control gains are applied at t=2 sec. FFT Analysis is used after the step change is implemented.

high validity. Therefore, this study analyzes the sensitivity of vector current control and PLL structure in a non-linear grid-following converter model with high accuracy; it can be the basis for future research on more complex control topologies as well as on studying the sensitivity analysis of small-signal model in different operating conditions.

ACKNOWLEDGMENT

This project has received funding from the European Union's Horizon 2020 research and innovation programme under the Marie Sklodowska-Curie grant agreement No 861398.

REFERENCES

[1] Wind Energy in Europe: 2021 Statistics and the outlook for 2022-2026. Available: https://windeurope.org/intelligence-platform/product/wind-energy-in-europe-2021-statistics-and-the-outlook-for-2022-2026/.

[2] X. Wang and F. Blaabjerg, "Harmonic Stability in Power Electronic-Based Power Systems: Concept, Modeling, and Analysis," in IEEE Transactions on Smart Grid, vol. 10, no. 3, pp. 2858-2870, May 2019

[3] X. Wang, M. G. Taul, H. Wu, Y. Liao, F. Blaabjerg and L. Harnefors, "Grid-Synchronization Stability of Converter-Based Resources—An Overview," in IEEE Open Journal of Industry Applications, vol. 1, pp. 115-134, 2020

[4] N. Kroutikova, C. Hernandez-Aramburo, and T. Green, "State-space model of grid-connected inverters under current control mode," in IEEE Transactions on Industrial Electronics, vol. 1, no. 3, pp. 329–338, May 2007

[5] A. Egea-Alvarez, S. Fekriasl, F. Hassan and O. Gomis-Bellmunt, "Advanced Vector Control for Voltage Source Converters Connected to Weak Grids," in IEEE Transactions on Power Systems, vol. 30, no. 6, pp. 3072-3081, Nov. 2015

[6] Y. Wang, X. Wang, F. Blaabjerg and Z. Chen, "Harmonic Instability Assessment Using State-Space Modeling and Participation Analysis in Inverter-Fed Power Systems," in IEEE Transactions on Industrial Electronics, vol. 64, no. 1, pp. 806-816, Jan. 2017

[7] G. S. Misyris, J. A. Mermet-Guyennet, S. Chatzivasileiadis and T. Weckesser, "Grid Supporting VSCs in Power Systems with Varying Inertia and Short-Circuit Capacity," proc. of 2019 IEEE Milan PowerTech, 2019, pp. 1-6

[8] M. Amin, J. A. Suul, S. D'Arco, E. Tedeschi and M. Molinas, "Impact of state-space modelling fidelity on the small-signal dynamics of VSC-HVDC systems," proc. of 11th IET International Conference on AC and DC Power Transmission, 2015, pp. 1-11

[9] F. Cecati, R. Zhu, M. Liserre and X. Wang, "Nonlinear Modular State-Space Modeling of Power-Electronics-Based Power Systems," in IEEE Transactions on Power Electronics, vol. 37, no. 5, pp. 6102-6115, May 2022

[10] L. Marin, A. Tarrasó, I. Candela and P. Rodriguez, "Stability Analysis of a Droop-Controlled Grid-Connected VSC," proc. of 2018 IEEE Energy Conversion Congress and Exposition (ECCE), 2018, pp. 4161-4167

[11] D. Yang and X. Wang, "Unified Modular State-Space Modeling of Grid-Connected Voltage-Source Converters," in IEEE Transactions on Power Electronics, vol. 35, no. 9, pp. 9700-9715, Sept. 2020

[12] F. Mandrile, S. Musumeci, E. Carpaneto, R. Bojoi, T. Dragičević, and F. Blaabjerg, "State-space modeling techniques of emerging grid connected converters," Energies, vol. 13, no. 18, p. 4824, Sep. 2020